Journal of Power Sources 196 (2011) 9369–9372

Contents lists available at ScienceDirect

Journal of Power Sources

journal homepage: www.elsevier.com/locate/jpowsour

Short communication

Enhanced formic acid oxidation on Cu–Pd nanoparticles

Lin Dai, Shouzhong Zou*

Department of Chemistry and Biochemistry, Miami University, Oxford, OH 45056, USA

ARTICLE INFO

Article history:
Received 11 June 2011
Received in revised form 30 July 2011
Accepted 2 August 2011
Available online 9 August 2011

Keywords:
Copper–palladium alloy nanoparticles
Formic acid oxidation
Electrocatalysts
Fuel cells

ABSTRACT

Developing catalysts with high activity and high resistance to surface poisoning remains a challenge in direct formic acid fuel cell research. In this work, copper–palladium nanoparticles were formed through a galvanic replacement process. After electrochemically selective dissolution of surface Cu, Pd-enriched Cu–Pd nanoparticles were formed. These particles exhibit much higher formic acid oxidation activities than that on pure Pd nanoparticles, and they are much more resistant to the surface poisoning. Possible mechanisms of catalytic activity enhancement are briefly discussed.

1. Introduction

Direct fuel cells using small organic compounds as liquid fuels are attractive power sources for portable electronic devices because these fuels are convenient to store, transport and refill, allowing for simple system design and cell operation. Among different choices, direct formic acid fuel cells (DFAFCs) have recently received much attention [1–3]. Compared to more extensively studied direct methanol fuel cells (DMFCs), DFAFCs are less sensitive to fuel crossover and have a higher theoretical voltage [2,3].

Both Pt and Pd have been frequently studied as catalyst materials for formic acid electrooxidation [4–10]. From studies on Pt electrodes, a dual pathway reaction mechanism has been proposed and widely recognized [4]. One path involves direct oxidation of formic acid to carbon dioxide (the so-called direct path) while another forms an inhibiting intermediate, most likely adsorbed carbon monoxide (CO_{ads}) produced from formic acid dehydration (indirect path) [4]. The CO_{ads} leads to severe poisoning of the catalyst surface. In comparison to Pt, Pd is known to catalyze the oxidation of formic acid through more facile direct path to form CO_2 and is less vulnerable to CO poisoning [11,12]. Nevertheless deactivation of Pd catalyst does occur [2,13,14].

Recent efforts in formic acid oxidation have been focused on increasing catalyst activity and durability through various approaches. It has been demonstrated that formic acid oxidation was more facile on Pd modified by a second element, such as Sn [15], Co [16], Pb [17], B [18], and P [19], than on pure Pd and the catalyst deactivation was much slower. The alloying effect can be largely understood in the frame work of the d-band theory [20]. The addition of the second element decreases the Pd d-band center and therefore weakens the adsorption of inhibiting reaction intermediates. Another approach involves the use of novel Pd nanostructures which exhibit higher formic acid oxidation activity [21–23].

Herein we report a new electrocatalyst that consists of Cu–Pd alloy nanoparticles (NPs) that were formed by depositing Pd on Cu NPs through galvanic redox reactions. After the surface Cu was selectively removed by electrochemical potential cycling, these new catalysts show a considerably higher activity for formic acid oxidation than pure Pd, and are much more resistant to surface poisoning.

2. Experimental

Cu NPs were prepared utilizing a modified method based on that reported by Wu and coworkers [24]. Briefly, 4.44 g of polyvinylpyrrolidone (PVP, MW 55,000) and 0.062 g of $CuSO_4 \cdot 5H_2O$ were dissolved in 40 mL of water. The obtained solution was purged with N_2 for approximately 1 h in order to remove dissolved O_2. Then 1.76 g of L-ascorbic acid (AA) was dissolved in 10 mL of deaerated water and added to the $CuSO_4$–PVP solution while the solution was stirred and protected with N_2. The temperature of the solution was then raised to around 50 °C and the reaction was allowed to proceed for 1 h to yield Cu NPs. The solution color changed from light blue to dark red within 10–15 min, indicating the formation of Cu NPs. Unlike Wu et al. [24], we found that it is necessary to purge the solution with N_2 during the whole process, otherwise no Cu NPs would form. It is known that AA is oxidized rapidly in the presence of heat and oxygen, and the reaction is catalyzed by Cu^{2+} [25].

* Corresponding author. Tel.: +1 513 5298084; fax: +1 513 5295715.
E-mail address: zous@muohio.edu (S. Zou).

0378-7753/$ – see front matter © 2011 Elsevier B.V. All rights reserved.
doi:10.1016/j.jpowsour.2011.08.004

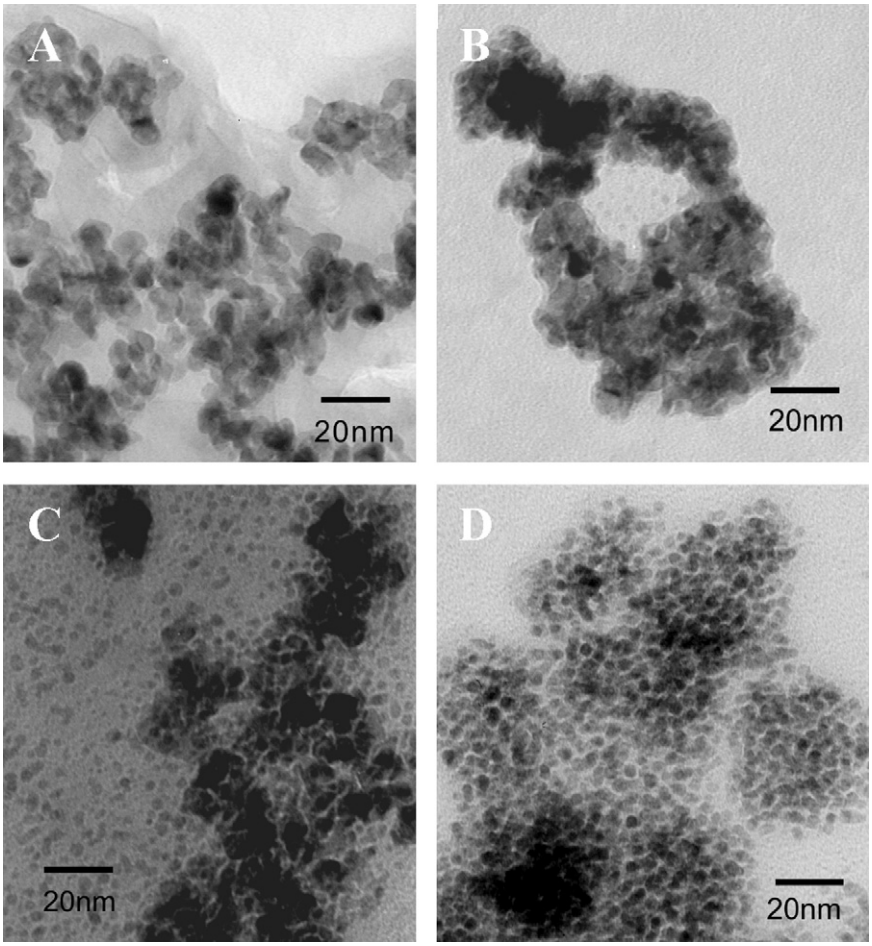

Fig. 1. TEM images of as prepared Cu–Pd NPs. (A) Pd_2Cu_7; (B) Pd_4Cu_7; (C) Pd_6Cu_7; (D) Pd_8Cu_7. Scale bar: 20 nm.

To form Cu–Pd NPs, 10 mL of room temperature Cu colloidal solution was added quickly into a deaerated K_2PdCl_4 solution and stirred for 1 h. N_2 protection during the reaction is essential to avoid oxidation of Cu NPs. Because the redox potential of $PdCl_4^{2-}$/Pd is higher than that of Cu^{2+}/Cu, Pd(II) is reduced to Pd and therefore Cu–Pd particles were formed [26]. To vary the Pd to Cu input atomic ratio, 5 mL Pd precursor solutions containing 5.5, 11.0, 16.5, and 22.0 mg of K_2PdCl_4 were used. These solutions contain amounts of Pd that are expected to cover Cu NPs with 1–4 nominal atomic layer of Pd, respectively, on the basis of the assumption that the Cu NPs are 4.5 nm spherical particles. The formed particles are denoted as Pd_2Cu_7, Pd_4Cu_7, Pd_6Cu_7 and Pd_8Cu_7 according to the input atomic ratio of Pd to Cu. Pure Pd NPs were synthesized following the same procedure of Cu NPs except that no $CuSO_4$ was used. Before microscopic and electrochemical measurements, the particles were washed with 1 M NaOH and ethanol by repetitive centrifugation and dispersion to remove the majority of PVP [27]. The cleaned particles were redispersed in the same volume of ethanol by sonication. The composition of Cu and Pd in the NPs was determined by using an inductively coupled plasma mass spectrometer (ICP-MS). The samples for determination of the Cu/Pd ratio before potential cycling were prepared by adding 10 μL of the synthesized nanoparticle suspension to a fresh aqua regia to dissolve the particles. For the determination of the Cu/Pd ratio after potential cycling, 10 μL of the same Cu–Pd nanoparticle suspension was drop-coated on a GC electrode and the nanoparticles were digested in fresh aqua regia overnight after the electrochemical measurements. The obtained solution was diluted 20 times by water before ICP-MS measurements. Transmission electron microscopy (TEM) images of washed particles without subject to potential cycling treatment were obtained using a Zeiss 10C microscope at an accelerating voltage of 100 kV.

To study the electrochemical behavior of these catalysts, cyclic voltammograms (CVs) and chronoamperograms (CAs) were recorded in 0.5 M HCOOH + 0.1 M $HClO_4$ in a conventional two-compartment three-electrode cell using a CHI 630 electrochemical analyzer. A Pt wire served as the counter electrode, and a KCl-saturated Ag/AgCl electrode was used as the reference electrode. However, the potentials are reported with respect to a reversible hydrogen electrode (RHE). The working electrode was prepared by drop-coating 10 μL of Cu–Pd suspension or Pd/C (20 wt%, Alfa Aesar) suspension (0.5 mg Pd/C per mL) in a water/ethanol (4:1 volume ratio) mixture on a glassy carbon (GC) disk electrode (geometric area: 0.196 cm^2) without using any binder, followed by 15 min 200 W Ar plasma treatment to remove residual organic protecting layers on the particle surfaces. The cell resistance was compensated with the iR compensation function in the analyzer. The Pd surface areas of the catalysts (including Pd/C) were determined electrochemically by CO stripping charge [18] assuming the charge for oxidation of a monolayer of adsorbed CO is 0.420 mC cm^{-2}. The CO adlayer was formed by sparging the gas in deaerated 0.1 M $HClO_4$ solution for 5 min followed by N_2 purging for 15 min with the electrode potential held at 0.25 V vs RHE. All of the solutions were prepared using water purified by a Milli-Q system with a resistivity of 18.2 MΩ cm. Measurements were made at room temperature (22 ± 1 °C).

Table 1
Cu–Pd nanoparticle composition and Pd loading.

	Pd_2Cu_7	Pd_4Cu_7	Pd_6Cu_7	Pd_8Cu_7
Cu:Pd ratio before PC	2.64	1.80	1.13	0.49
Cu:Pd ratio after PC	0.33	0.45	0.30	0.24
Pd loading after PC ($\mu g\,cm^{-2}$ GC electrode)	45.1	24.0	22.3	31.3

3. Results and discussion

The Cu–Pd NPs were formed by mixing $PdCl_4^{2-}$ with a Cu nanoparticle (NP) colloidal suspension. Because the equilibrium potential of $PdCl_4^{2-}$/Pd is higher than that of Cu^{2+}/Cu, Pd (II) is reduced by Cu and metallic Pd is deposited on Cu NP surface through a galvanic redox replacement process [26]. Fig. 1 displays TEM images of Cu–Pd NPs with varying input Cu/Pd atomic ratio as denoted in their respective notations. The deposition of Pd on Cu NPs is evident by the enhanced contrast in the TEM image; with pure Cu NPs, no clear particles can be seen with the electron microscope we used due to the lighter atomic weight of Cu (image not shown). With the increasing amount of $PdCl_4^{2-}$, more Pd is deposited on Cu particles as evident by the increased contrast from Fig. 1A to D. This conclusion is confirmed by the results from ICP-MS measurements summarized in Table 1. Significant particle aggregations were observed in some of the images. Nevertheless, individual particles can be identified, and their sizes were measured to be around 3–4 nm.

To examine their electrochemical behavior, these Cu–Pd NPs were drop-coated on a glassy carbon (GC) electrode after they were washed and redispersed in ethanol as described in Section 2. Fig. 2 displays selective CVs of Cu–Pd NPs on a GC electrode in 0.1 M $HClO_4$. Fig. 2A was obtained with Pd_4Cu_7 NPs. In the first positive scan, a large anodic current peak was observed at potentials between 0.3 and 0.7 V, signifying Cu oxidation and dissolution [28]. As the potential was scanned to higher values, a second current increase was seen at above 0.85 V which can be attributed to the oxidation of Pd surface. On the reverse potential scan, a reduction peak at around 0.7 V from the reduction of palladium oxides appeared, followed by a second reduction peak at 0.5 V attributable to reduction of copper oxides. At more negative potentials, a reduction peak showed up below 0.2 V, which arose from hydrogen adsorption/absorption on Pd. Upon successive potential scan, the Cu oxidation and corresponding oxide reduction current peaks gradually decreased, while the Pd oxidation and corresponding oxide reduction currents decrease only slightly. After about 15 cycles, the CVs were stable and resemble that from pure Pd NPs (Fig. 2B). The cyclic voltammetric transitions of other Cu–Pd particles are similar to those shown in Fig. 2A, albeit the shape and position of Cu related current peaks varied slightly. Selective examples of stable CVs of different Cu–Pd NPs are demonstrated in Fig. 2B. The oxide formation and removal peaks are similar to those from pure Pd NPs. These observations suggest that the Cu–Pd NPs initially do not have a core-shell structure. However after selective dissolution of Cu, the particle surface is enriched with Pd. The loss of Cu in the particles was confirmed by the significant decrease of Cu to Pd molar ratio obtained from the ICP-MS measurements after the potential cycling (PC) treatment (Table 1). The dissolution of Pd during potential cycling is negligible as evident by nearly identical amounts of Pd in samples with and without subject to the PC determined by ICP-MS. The Pd loadings of Cu–Pd nanoparticles after PC treatment are summarized in Table 1.

After stable CVs were obtained, the catalytic activity of these Cu–Pd NPs was examined in a 0.5 M HCOOH + 0.1 M $HClO_4$ solution. Fig. 3A shows selective CVs of formic acid oxidation on Cu–Pd NPs. For comparison, results from a commercially available Pd/C were also included. The current density was calculated by normalizing the obtained current to the electrochemically active Pd surface area assessed by using CO stripping charge as described in Section 2. A current peak was observed at around 0.55 V from both potential scan directions for all of the samples. Clearly the Cu–Pd NPs show a much higher current density from 0.10 to 0.75 V, indicating they are more active for formic acid oxidation than pure Pd NPs. The enhanced formic acid oxidation catalytic activity depends on the original particle composition. The peak current density from Pd_6Cu_7 is about 10 times of that from Pd/C and 1.8 times of that from Pd_8Cu_7. The peak current density of other Cu–Pd NPs is lower than the two Cu–Pd samples, but higher than Pd/C. Similar enhanced formic acid oxidation on porous CuPd alloys formed by dealloying PdCuAl ternary alloys was recently reported [29].

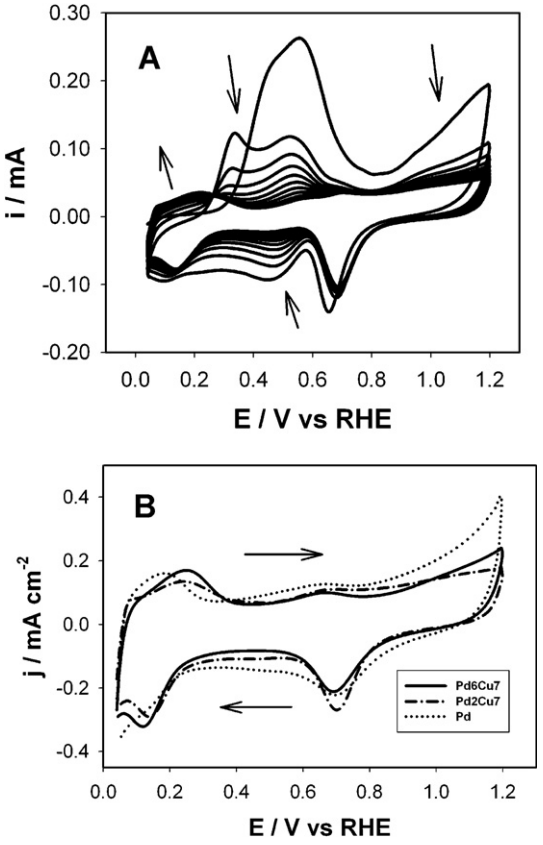

Fig. 2. (A) CVs of Pd_4Cu_7 supported on a GC electrode obtained in 0.1 M $HClO_4$. (B) Stable CVs of Pd_2Cu_7, Pd_6Cu_7 and pure Pd NPs supported on GC electrodes. Scan rate: 0.100 V s^{-1}. The arrows indicate the current changes in (A) and scan directions in (B).

The enhanced formic acid oxidation activity of Cu–Pd NPs was further confirmed by the chronoamperometric (CA) measurements at 0.25 V shown in Fig. 3B. The steady state current density for all of the Cu–Pd NPs is significantly higher than that from Pd/C, and depends on the initial particle composition. The catalytic activity of Cu–Pd is the highest on Pd_6Cu_7, followed by Pd_8Cu_7, then Pd_4Cu_7, and Pd_2Cu_7 has the lowest activity enhancement. The activity loss on these catalysts is related to their initial compositions as well. The half life of the activity, defined as the time when the current density decreases by 50%, is 210 s for Pd_6Cu_7, 130 s for Pd_8Cu_7, 60 s for Pd_4Cu_7, 10 s for Pd_2Cu_7 and less than 5 s for Pd/C (Fig. 3B inset). At the end of the measurements, the current density on Pd_6Cu_7 is 36 times of that on Pd/C. The significant activity and stability improvement of Cu–Pd NPs over Pd/C is also evident in their mass activity measurements. For example, at 1000 s and 0.25 V the mass activity on Pd_8Cu_7 is 12 mA mg^{-1} Pd while on Pd/C it is 0.18 mA mg^{-1} Pd.

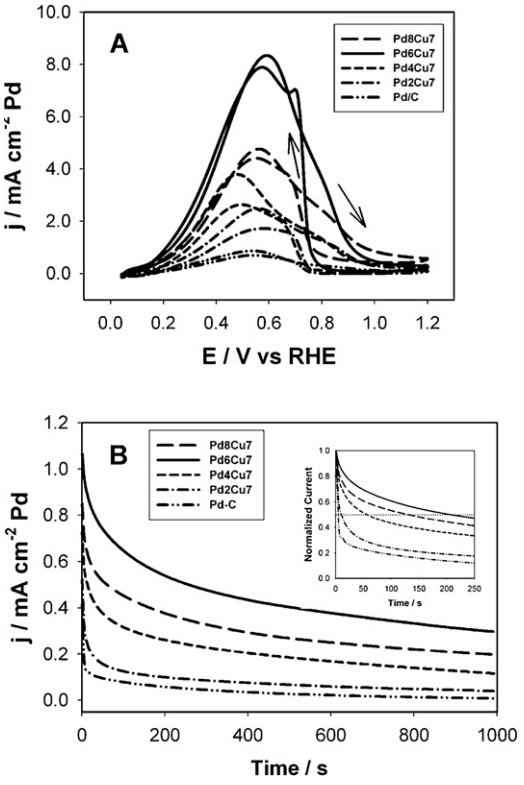

Fig. 3. (A) CVs of formic acid oxidation on various catalysts obtained in deaerated 0.5 M HCOOH and 0.1 M $HClO_4$. Scan rate: 0.100 V s^{-1}. The arrows indicate the potential scan direction. (B) Chronoamperometric plots of formic acid oxidation on various catalysts at 0.250 V (vs RHE) in deaerated 0.5 M HCOOH and 0.1 M $HClO_4$. Initial potential: 0.050 V. Inset: plots of normalized current vs time.

It is generally accepted that formic acid oxidation on Pt-group transition metals occurs through two pathways [4]: the direct pathway in which HCOOH is oxidized to CO_2 through a reactive intermediate (or intermediates) whose identity is still under active debate [6,30,31], and the indirect pathway where HCOOH undergoes dehydration to form strongly adsorbed CO which poisons the catalyst surfaces. Consequently, there are two related approaches to promote formic acid oxidation: enhancing the direct pathway or decreasing the CO poisoning effect. After the PC treatment the Cu–Pd NP surfaces are enriched with Pd, as suggested by the resemblance of their CVs to that of pure Pd NPs (Fig. 2B). The enhanced formic acid oxidation activity also supports that the particle surface is rich in Pd, as the presence of Cu on Pd would block the active sites [32]. There are significant amounts of Cu left in the particles (Table 1) that are buried underneath the Pd layer. Based on the d-band theory, the presence of Cu would lower the Pd d-band center position and therefore weaken the CO adsorption [20]. This effect will delay the CO poisoning on Cu–Pd NPs therefore retain the high activity of Pd for formic acid oxidation. This explanation corroborates with the chronoamperometric results shown in Fig. 3B, which reveals that the half life of catalytic activity of formic acid oxidation on Cu–Pd is much prolonged as compared to that on Pd/C. The weakening of CO adsorption has previously been reported on Pt_3Co nanocubes[33] and other Pt–M alloys [34]. Fouda-Onana et al. showed by DFT calculations that the d-band center of Cu–Pd alloys decreases with increasing Cu content [35]. It has also been shown in ultra high vacuum that CO adsorption on PdCu alloys is weaker than on pure Pd due to the decrease of d-band center [36,37]. In addition to the weakening of CO poisoning effect, the enhanced catalytic activity on Cu–Pd may also come from the formation of more active sites by dissolution of Cu from the particle surfaces, as have been reported on several porous Pd nanostructures [21,38]. This effect may arise from the fact that formic acid oxidation is surface structure sensitive, as demonstrated by using Pd single crystal surfaces [7,11].

4. Conclusions

In summary, we showed that Cu–Pd NPs with different compositions were formed by addition of Pd salt into a Cu NP colloidal solution. After a potential cycling treatment to selectively remove surface Cu, Pd enriched Cu–Pd NPs were formed. Compared to the commercially available Pd/C catalysts, significantly higher and much more stable formic acid oxidation activities were observed on Cu–Pd particles. These particles are promising anode catalysts for direct formic acid fuel cells.

Acknowledgment

This work was partially supported by NSF (CHM-0616436).

References

[1] C. Rice, S. Ha, R.I. Masel, P. Waszczuk, A. Wieckowski, T.M. Barnard, J. Power Sources 111 (2002) 83–89.
[2] X.W. Yu, P.G. Pickup, J. Power Sources 182 (2008) 124–132.
[3] S. Uhm, H.J. Lee, J. Lee, Phys. Chem. Chem. Phys. 11 (2009) 9326–9336.
[4] A. Capon, R. Parsons, J. Electroanal. Chem. 44 (1973) 1.
[5] A. Capon, R. Parsons, J. Electroanal. Chem. 44 (1973) 239.
[6] Y.X. Chen, M. Heinen, Z. Jusys, R.J. Behm, Angew. Chem.-Int. Edit. 45 (2006) 981–985.
[7] N. Hoshi, M. Nakamura, K. Kida, Electrochem. Commun. 9 (2007) 279–282.
[8] R. Larsen, S. Ha, J. Zakzeski, R.I. Masel, J. Power Sources 157 (2006) 78–84.
[9] G.Q. Lu, A. Crown, A. Wieckowski, J. Phys. Chem. B 103 (1999) 9700–9711.
[10] S. Park, Y. Xie, M.J. Weaver, Langmuir 18 (2002) 5792–5798.
[11] N. Hoshi, K. Kida, M. Nakamura, M. Nakada, K. Osada, J. Phys. Chem. B 110 (2006) 12480–12484.
[12] W.P. Zhou, A. Lewera, R. Larsen, R.I. Masel, P.S. Bagus, A. Wieckowski, J. Phys. Chem. B 110 (2006) 13393–13398.
[13] S. Ha, R. Larsen, Y. Zhu, R.I. Masel, Fuel Cells 4 (2004) 337–343.
[14] Y.M. Zhu, Z. Khan, R.I. Masel, J. Power Sources 139 (2005) 15–20.
[15] Z.H. Zhang, J.J. Ge, L.A. Ma, J.H. Liao, T.H. Lu, W. Xing, Fuel Cells 9 (2009) 114–120.
[16] D. Morales-Acosta, J. Ledesma-Garcia, L.A. Godinez, H.G. Rodriguez, L. Alvarez-Contreras, L.G. Arriaga, J. Power Sources 195 (2010) 461–465.
[17] R.S. Li, H. Hao, W.B. Cai, T. Huang, A.S. Yu, Electrochem. Commun. 12 (2010) 901–904.
[18] J.Y. Wang, Y.Y. Kang, H. Yang, W.B. Cai, J. Phys. Chem. C 113 (2009) 8366–8372.
[19] L.L. Zhang, Y.W. Tang, J.C. Bao, T.H. Lu, C. Li, J. Power Sources 162 (2006) 177–179.
[20] J.R. Kitchin, J.K. Nørskov, M.A. Barteau, J.G. Chen, J. Chem. Phys. 120 (2004) 10240.
[21] C.Y. Du, M. Chen, W.G. Wang, G.P. Yin, ACS Appl. Mater. Interfaces 3 (2011) 105–109.
[22] V. Mazumder, S.H. Sun, J. Am. Chem. Soc. 131 (2009) 4588–4589.
[23] Y. Yu, Q.B. Zhang, B. Liu, J.Y. Lee, J. Am. Chem. Soc. 132 (2010) 18258–18265.
[24] C. Wu, B.P. Mosher, T. Zeng, J. Nanoparticle Res. 8 (2006) 965–969.
[25] V. Kuellmer, Kirk-Othmer Concise Encyclopedia of Chemical Technology, John Wiley and Sons, 2007.
[26] S.R. Brankovic, J.X. Wang, R.R. Adzic, Surf. Sci. 474 (2001) 173–179.
[27] C. Susut, G.B. Chapman, G. Samjesk, M. Osawa, Y.Y. Tong, Phys. Chem. Chem. Phys. 10 (2008) 3712–3721.
[28] S. Koh, P. Strasser, J. Am. Chem. Soc. 129 (2007) 12624–12625.
[29] C. Xu, H. Qiu, Y. Liu, Electrochem. Commun. (2011), doi:10.1016/j.elecom.2011.04.007.
[30] Y.X. Chen, S. Ye, M. Heinen, Z. Jusys, M. Osawa, R.J. Behm, J. Phys. Chem. B 110 (2006) 9534–9544.
[31] W. Gao, J.A. Keith, J. Anton, T. Jacob, J. Am. Chem. Soc. 132 (2010) 18377–18385.
[32] K. Brandt, M. Steinhausen, K. Wandelt, J. Electroanal. Chem. 616 (2008) 27–37.
[33] H.Z. Yang, J. Zhang, K. Sun, S.Z. Zou, J.Y. Fang, Angew. Chem.-Int. Edit. 49 (2010) 6848–6851.
[34] H. Uchida, K. Izumi, K. Aoki, M. Watanabe, Phys. Chem. Chem. Phys. 11 (2009) 1771–1779.
[35] F. Fouda-Onana, S. Bah, O. Savadogo, J. Electroanal. Chem. 636 (2009) 1–9.
[36] T. Hager, H. Rauscher, R.J. Behm, Surf. Sci. 558 (2004) 181–194.
[37] A. Hammoudeh, J. Loboda-Cackovic, M.S. Mousa, J.H. Block, Vacuum 48 (1997) 187–190.
[38] X.G. Wang, W.M. Wang, Z. Qi, C.C. Zhao, H. Ji, Z.H. Zhang, Electrochem. Commun. 11 (2009) 1896–1899.